Extremely sub-wavelength THz metal-dielectric wire microcavities

Cheryl Feuillet-Palma,[1] Yanko Todorov,[1,*] Robert Steed,[1] Angela Vasanelli,[1] Giorgio Biasiol,[2] Lucia Sorba,[3] and Carlo Sirtori[1]

[1]*Univ. Paris Diderot, Sorbonne Paris Cité, Laboratoire Matériaux et Phénomènes Quantiques, UMR7162, 75013 Paris, France*

[2]*IOM CNR, Laboratorio TASC, Area Science Park, I-34149 Trieste, Italy*

[3] *NEST, Istituto Nanoscienze-CNR and Scuola Normale Superiore, I-56127 Pisa, Italy*

[*]*yanko.todorov@univ-paris-diderot.fr*

Abstract: We demonstrate minimal volume wire THz metal-dielectric micro-cavities, in which all but one dimension have been reduced to highly sub-wavelength values. The smallest cavity features an effective volume of 0.4 μm^3, which is ~5.10^{-7} times the volume defined by the resonant vacuum wavelength (λ = 94 μm) to the cube. When combined with a doped multi-quantum well structure, such micro-cavities enter the ultra-strong light matter coupling regime, even if the total number of electrons participating to the coupling is only in the order of 10^4, thus much less than in previous studies.

OCIS codes: (140.3945) Microcavities; (050.6624) Subwavelength structures; (130.5990) Semiconductors; (260.3090) Infrared, far; (270.5580) Quantum electrodynamics.

References and links

1. J. B. Pendry, A. J. Holden, D. J. Robbins, and W. J. Stewart, "Magnetism from Conductors, and Enhanced Non-Linear Phenomena," IEEE Trans. Microw. Theory Tech. **47**(11), 2075–2084 (1999).
2. M. W. Klein, C. Enkrich, M. Wegener, C. M. Soukoulis, and S. Linden, "Single-slit split-ring resonators at optical frequencies: limits of size scaling," Opt. Lett. **31**(9), 1259–1261 (2006).
3. E. Strupiechonski, G. Xu, N. Isac, M. Brekenfeld, Y. Todorov, A. M. Andrews, C. Sirtori, G. Strasser, A. Degiron, and R. Colombelli, "Sub-diffraction-limit semiconductor resonators operating on the fundamental magnetic resonance," Appl. Phys. Lett. **100**(13), 131113 (2012).
4. V. M. Shalaev, "Optical negative-index metamaterials," Nat. Photonics **1**(1), 41–48 (2007).
5. J. B. Pendry, L. Martín-Moreno, and F. J. Garcia-Vidal, "Mimicking Surface Plasmons with Structured Surfaces," Science **305**(5685), 847–848 (2004).
6. S. A. Maier, "Plasmonic field enhancement and SERS in the effective mode volume picture," Opt. Express **14**(5), 1957–1964 (2006).
7. P. Biagioni, J.-S. Huang, and B. Hecht, "Nanoantennas for visible and infrared radiation," Rep. Prog. Phys. **75**(2), 024402 (2012).
8. M. J. Adams, *An Introduction to Optical Waveguides*, (John Wiley & Sons, Chichester, 1981).
9. A. P. Hibbins, J. R. Sambles, C. R. Lawrence, and J. R. Brown, "Squeezing Millimeter Waves into Microns," Phys. Rev. Lett. **92**(14), 143904 (2004).
10. Y. Todorov, L. Tosetto, J. Teissier, A. M. Andrews, P. Klang, R. Colombelli, I. Sagnes, G. Strasser, and C. Sirtori, "Optical properties of metal-dielectric-metal microcavities in the THz frequency range," Opt. Express **18**(13), 13886–13907 (2010).
11. P. Jouy, Y. Todorov, A. Vasanelli, R. Colombelli, I. Sagnes, and C. Sirtori, "Coupling of a surface plasmon with localized subwavelength microcavity modes," Appl. Phys. Lett. **98**(2), 021105 (2011).
12. C. Ciuti, G. Bastard, and I. Carusotto, "Quantum vacuum properties of the intersubband cavity polariton field," Phys. Rev. B **72**(11), 115303 (2005).
13. Y. Todorov, A. M. Andrews, R. Colombelli, S. De Liberato, C. Ciuti, P. Klang, G. Strasser, and C. Sirtori, "Ultrastrong Light-Matter Coupling Regime with Polariton Dots," Phys. Rev. Lett. **105**(19), 196402 (2010).
14. P. Jouy, A. Vasanelli, Y. Todorov, A. Delteil, G. Biasiol, L. Sorba, and C. Sirtori, "Transition from strong to ultrastrong coupling regime in mid-infrared metal-dielectric-metal cavities," Appl. Phys. Lett. **98**(23), 231114 (2011).
15. M. Geiser, F. Castellano, G. Scalari, M. Beck, L. Nevou, and J. Faist, "Ultrastrong Coupling Regime and Plasmon Polaritons in Parabolic Semiconductor Quantum Wells," Phys. Rev. Lett. **108**(10), 106402 (2012).

#178514 - $15.00 USD Received 23 Oct 2012; revised 5 Dec 2012; accepted 5 Dec 2012; published 14 Dec 2012

16. C. Ciuti and I. Carusotto, "Input-output theory of cavities in the ultrastrong coupling regime: The case of time-independent cavity parameters," Phys. Rev. A **74**(3), 033811 (2006).
17. S. De Liberato and C. Ciuti, "Quantum theory of electron tunneling into intersubband cavity polariton states," Phys. Rev. B **79**(7), 075317 (2009).
18. U. Rössler, *Solid State Theory*, (Springer, 2009).
19. T. Atay, J.-H. Song, and A. V. Nurmikko, "Strongly interacting plasmon nanoparticle pairs: from dipole–dipole interaction to conductively coupled regime," Nano Lett. **4**(9), 1627–1631 (2004).
20. M. Helm, in *Intersubband Transitions in Quantum Wells: Physics and Device Applications I,* H. C. Liu, F. Capasso, eds. (Academic Press, 2000).
21. S. Zanotto, R. Degl'Innocenti, L. Sorba, A. Tredicucci, and G. Biasiol, "Analysis of line shapes and strong coupling with intersubband transitions in one-dimensional metallodielectric photonic crystal slabs," Phys. Rev. B **85**(3), 035307 (2012).
22. E. Peter, P. Senellart, D. Martrou, A. Lemaître, J. Hours, J. M. Gérard, and J. Bloch, "Exciton-Photon Strong-Coupling Regime for a Single Quantum Dot Embedded in a Microcavity," Phys. Rev. Lett. **95**(6), 067401 (2005).
23. H. T. Miyazaki and Y. Kurokawa, "Squeezing visible light waves into a 3-nm-thick and 55-nm-long plasmon cavity," Phys. Rev. Lett. **96**(9), 097401 (2006).
24. E. M. Purcell, H. Torrey, and R. Pound, "Resonance Absorption by Nuclear Magnetic Moments in a Solid," Phys. Rev. **69**(1-2), 674 (1946).
25. C. Walther, G. Scalari, M. Beck, and J. Faist, "Purcell effect in the inductor-capacitor laser," Opt. Lett. **36**(14), 2623–2625 (2011).
26. Y. Todorov, I. Sagnes, I. Abram, and C. Minot, "Purcell Enhancement of Spontaneous Emission from Quantum Cascades inside Mirror-Grating Metal Cavities at THz Frequencies," Phys. Rev. Lett. **99**(22), 223603 (2007).
27. P. W. C. Hon, A. A. Tavallaee, Q.-S. Chen, B. S. Williams, and T. Itoh, "Radiation Model for Terahertz Transmission-Line Metamaterial Quantum-Cascade Lasers," IEEE Trans. THz Sci. Technol. **2**(3), 323–332 (2012).

1. Introduction

Recently, there have been numerous demonstrations of photonic resonators able to confine the light in volumes that are much smaller than the free space wavelength λ. All these resonators are commonly based on metals, but fall into two big categories. The prototype of the first category is the split-ring resonator [1–3], used as unit cell for meta-materials [4]. Such resonator basically acts as an electronic *LC* circuit [2], in which there is no wavelength cut- off, as the displacement current arising from the time varying electric field is negligible in this case. The second type of resonator relies on propagation effects. In this case the resonant condition is set by the round trip of a photon bouncing between two boundaries, while in one or both directions perpendicular to light propagation metallic (or plasmonic) boundary conditions permit to shrink the extension of the electromagnetic field in a very sub-wavelength scale [5–7].

In particular, double-metal microcavities are able to support modes that are highly sub-wavelength with respect to the distance between the metal layers [8]. This is often exploited in the microwave frequency range to fabricate waveguides and patch antennas [9]. Similar structures have been used at terahertz frequencies and in the mid-infrared [10, 11]. The reflectivity spectra from arrays of such microcavities display deep reflection minima at resonance frequencies, indicating their ability to strongly absorb an incoming electromagnetic fields regardless its incident direction [10]. For these experiments, typically square shaped micro-cavities were used, consisting of a metallic back-plane, a dielectric layer and a top metal layer which is patterned into square patches. Each cavity support separate confined TM_{nm0} modes. The fundamental resonance for this system corresponds to two degenerate modes, the TM_{010} and TM_{100}. The resonance condition is imposed by the side *s* of the square, which is approximately equal to $\lambda/2n$, where λ is the resonant wavelength, and *n* is the refractive index of the dielectric core. The typical thickness *L* of the core is, however, much smaller than the wavelength, $L << \lambda$.

The sub-wavelength confinement of the light field between the metal layers was exploited to reach the light-matter ultra-strong coupling regime [12] in the THz and MIR frequency range [13–15]. For these studies, the gap between the metal is filled with doped quantum wells (QWs) displaying a strong intersubband absorption. In this case, the light-matter

#178514 - $15.00 USD Received 23 Oct 2012; revised 5 Dec 2012; accepted 5 Dec 2012; published 14 Dec 2012

interaction is enhanced by the strongly subwavelength volume of the resonator V, as the coupling constant $2\Omega_R$, the Rabi splitting, increases as $2\Omega_R \sim\sqrt{N_e / V}$, where N_e is the number of electrons in the cavity. Electro-optic devices based on the strong coupling regime are expected to provide an increased radiative efficiency as the characteristic time of the Rabi oscillations, $T_R = 2\pi/\Omega_R$ is much faster than the typical spontaneous emission time [16]. However, the obstacle for achieving a device with an increased electro-optic conversion are the so called "dark" states [17], which have a quantum degeneracy equal to the number of electrons N_e in the device, while there are only two bright states corresponding to the polaritons. The injection probability for each bright state is therefore on the order of $1/N_e$, which is a very low number since in a typical microcavity $N_e \sim 10^5$. A possible approach to circumvent this problem is to use the smallest possible cavity volume V, so that the ratio N_e/V is preserved but with a reduced number of electrons N_e.

In this paper we report on a minimal volume wire cavity resonators in the THz spectral region. These structures are similar to the patch cavities reported in Ref [10], however now two dimensions of the resonators have been shrunk to highly sub-wavelength values, and only the length of the resonator s is kept equal to $\lambda/2n$. For the smallest of these devices the ratio V/λ^3 is $\sim 5.10^{-7}$, with the resonant vacuum wavelength $\lambda = 95$ μm. Furthermore, we have used these wire cavities to study the light-matter strong coupling regime. The comparison with square patch cavities shows that the Rabi splitting is not reduced in the wire resonators, while the total number of electrons in the system is reduced by more than an order of magnitude.

2. Wire microcavities

The wire microcavites are presented in Fig. 1. Figure 1(a) schematizes the geometry of a single microcavity, which consists of dielectric (GaAs) layer with thickness L, wafer-bonded on a gold-coated surface. A thin metallic stripe with length s and width w is deposited on the dielectric, with $s >> w$. The length s sets the resonant frequency of the fundamental mode TM_{100} through the formula:

$$v = \frac{c}{2n_{eff}s} \tag{1}$$

In this formula, c is the speed of light, and n_{eff} is the effective index of the mode, that depends both on the modal guided index of the wire-semiconductor-metal waveguide, and the phase of the effective reflectivity at the open ends of the resonator [10]. As it will be shown further in the text, the typical values of n_{eff} are close to the bulk GaAs index in the THz domain ($\lambda \sim 100$ μm), $n = 3.55$. In order to obtain resonances in the THz range, the typical strip length is $s \sim 10$ μm, while the other dimensions are kept very sub-wavelength: w, $L < 1$ μm. Figure 1(b) shows a dense periodic array of such structures. Nanofabrication has been be carried out using an electron beam lithography facility which includes a laser interferometer controlled stage for ensuring tenth of nanometer precision over millimeter length scales. The overall sample surface is 2x2 mm^2. Figures 1(c)-1(f) show the vertical component of the electric field (E_z) of the fundamental TM_{100} cavity resonance, for a thickness $L = 1$ μm (Figs. 1(c,d)) and $L = 300$ nm (Figs. 1(e,f)) in the (x,z) and (y,z) plane. These simulations were performed with the COMSOL finite element commercial software which resolves for the electromagnetic eigenmodes of the structure. The metallic layers are described with a frequency independent complex refractive index $150 + 250i$ and the semiconductor layers with an index 3.55. As expected, the field is strongly confined between the two metals, and displays a standing wave-like pattern along the strip, $E_z \sim \cos(x\pi/s)$. In the case of the $L = 1$ μm structure, there is a partial leakage in the air and a slight spreading in the y-direction (Figs. 1(c,d)). In the case of the $L = 300$ nm structure the vertical electric field E_z is quasi homogeneous in the two directions perpendicular to the stripe (y, z). In this case the expression for the effective volume is the geometrical volume of the structure, $V = swL = \lambda wL/(2n_{eff})$. We will

#178514 - $15.00 USD Received 23 Oct 2012; revised 5 Dec 2012; accepted 5 Dec 2012; published 14 Dec 2012

experimentally demonstrate that this formula is a very good approximation also for thicker structures, despite the partial leak in the air and the fringing fields around the resonator corners.

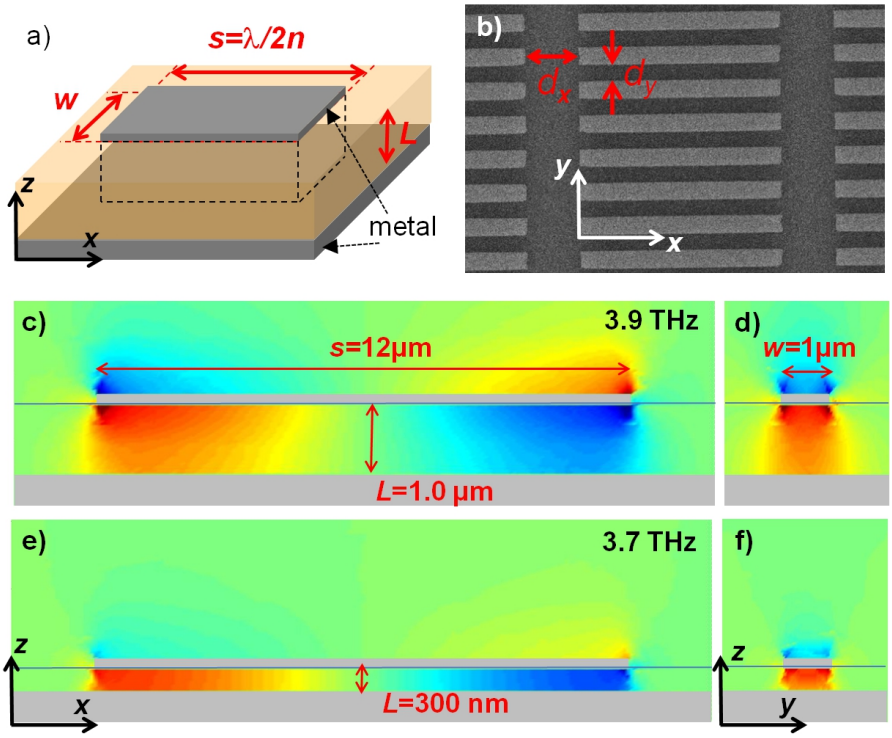

Fig. 1. (a) Schematics of a wire microcavity with the relevant geometrical dimensions. The structure consists of dielectric (typically GaAs) layer, bonded on a gold surface. A thin strip of gold is deposited on the top of the dielectric to complete the microcavity. (b) Scanning Electron Microscope (SEM) image of the top surface of an array of microcavities, with typical dimensions s = 12 μm, w = 1 μm and L = 1 μm. The relevant dimensions of the array are also indicated. (c), (d) Finite element simulations of the vertical electric field, for a microcavity with a thickness L = 1 μm. (e), (f), Vertical electric field for the fundamental resonance of a microcavity with a thickness L = 300 nm. In (c) and (e) we have indicated the corresponding computed eigenfrequencies for each structure.

To probe experimentally the microcavity resonances, we have performed reflectivity measurements on dense arrays of structures as those shown in Fig. 1(b). In our setup a polarized beam from a Globar lamp of a Bruker interferometer (IFS66) is focused on the sample and the reflected intensity is measured with a cooled Bolometer detector. The incident angle was either 10° or 45°. The absolute reflectivity is obtained by dividing the spectra on a reference obtained from unpatterned gold mirror. The parameters of the arrays, as defined in Fig. 1(b) were d_x = 5 μm and d_y = 2 μm. The unit cell of the array is $\Sigma = (d_x + s)\text{x}(d_y + w)$ = 51 μm^2 and remains very sub-wavelength. The only propagating diffracted order is therefore the 0th order, corresponding to the specular reflection. Such dense arrays allow increasing the contrast of the reflectivity dips that correspond to the resonant excitation of the cavity modes [10]. The results of the measurements, performed with four different microcavities, are reported in Fig. 2. The polarization of the incident light was chosen so that the electric field of the incident beam is parallel to the wires, and the incident angle was 10° for Fig. 2(a) and 45° for Fig. 2(b). The length of the stripe was fixed to s = 12 μm, and two sets of samples with different thickness L were used, L = 1 μm and L = 300 nm. In Fig. 2(a) we report the reflectivity results with a lateral dimension of w = 1 μm, while in Fig. 2(b) we have w = 100

#178514 - $15.00 USD Received 23 Oct 2012; revised 5 Dec 2012; accepted 5 Dec 2012; published 14 Dec 2012

nm. In Fig. 2(b), the higher incident angle (45°) for the w = 100 nm wires allowed for a further improvement of the contrast of the reflectivity features, as the contrast increases with the incident angle [10].

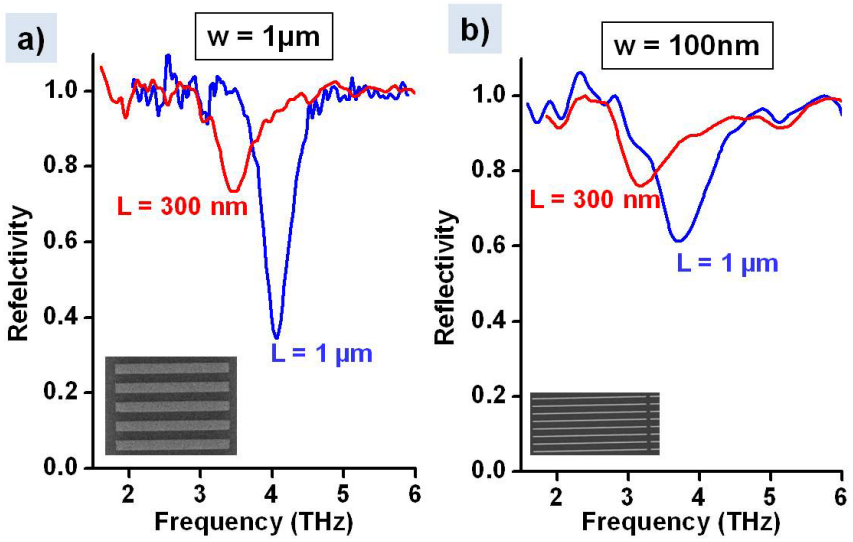

Fig. 2. Reflectivity spectra for cavities with s = 12 µm and various strip widths w, for core thicknesses L = 1 µm and L = 300 nm. a) w = 1 µm b) w = 100 nm. The insets in (a) and (b) show SEM pictures of the microcavity arrays employed in the experiments.

All the spectra clearly display the resonant reflectivity dip that corresponds to the excitation of the fundamental TM_{100} cavity mode as described in Fig. 1. The resonance frequencies for the thinner (L = 300 nm) structures is around 3.5 THz, and equal to 4 THz for the L = 1 µm structures. These values agree very well with the eigenvalues provided by the finite element method: 3.7 THz and 3.9 THz respectively, that correspond to the contour plots in Figs. 1(c-f). Considerable broadening of the reflectivity dips is observed for the micro-cavites with a width of w = 100 nm. Nevertheless, the clear reflectivity dip indicates that the mode is laterally confined by a strip width w which is 3 orders of magnitude smaller than the resonant wavelength. For the smallest structure (w = 100 nm and L = 300 nm) the incoming free-space photon with a wavelength λ = 100µm is squeezed in a volume V = 0.4 µm^3 that is 5.10^{-7} times the wavelength cubed λ^3.

As already seen in Fig. 1(d), the strong reduction of the y-lateral dimension of the stripe leads to spreading effects and an increase of the fringing fields. In order to investigate these effects, we have realized two sets of arrays, with thickness L = 300 nm and L = 1 µm, in which the lateral gap d_y between the wires is varied (see Fig. 1(b)). The gold stripe dimensions are kept constant: w = 1 µm and s = 12 µm. The separation d_x was also fixed to d_x = 3 µm. In Fig. 3(a), we report the measured resonant frequencies as a function of d_y and in Fig. 3(b) we plot the corresponding effective index n_{eff} from Eq. (1). We observe that the frequency increases up to d_y = 2µm and then remains constant. This behavior can be simply explained assuming the evanescent coupling between adjacent resonators in a tight binding model [18]. Similar trend has been observed with metallic nanoparticles in the visible, for separations larger than the conductive contact [19]. The frequency shift Δν is then proportional to the coupling constant that depends on the overlap between the evanescent tails of two adjacent cavities. This picture leads to an exponential law $\Delta\nu = \nu_\infty - (\nu_\infty - \nu_0)\exp(-d_y / d_0)$ where the values of ν_∞ and ν_0 correspond to the limit for d_y going towards ∞ and 0 respectively. The fit provides a typical length scale for the extension

#178514 - $15.00 USD Received 23 Oct 2012; revised 5 Dec 2012; accepted 5 Dec 2012; published 14 Dec 2012

of the exponential tails that is d_0 = 1.9 µm and d_0 = 1.3 µm for the L = 1 µm and L = 300 nm respectively. This result indicates that the fringing fields decrease as the thickness is reduced, as qualitatively observed in Fig. 1. Note that the asymptotic values of v_0 (2.7 THz for L = 300 nm, 3.2 THz for L = 1 µm) correspond to the resonant frequencies that would have been obtained for an infinite waveguide. Indeed in the limit d_y = 0 all wires merge together into an infinite stripe of a width s.

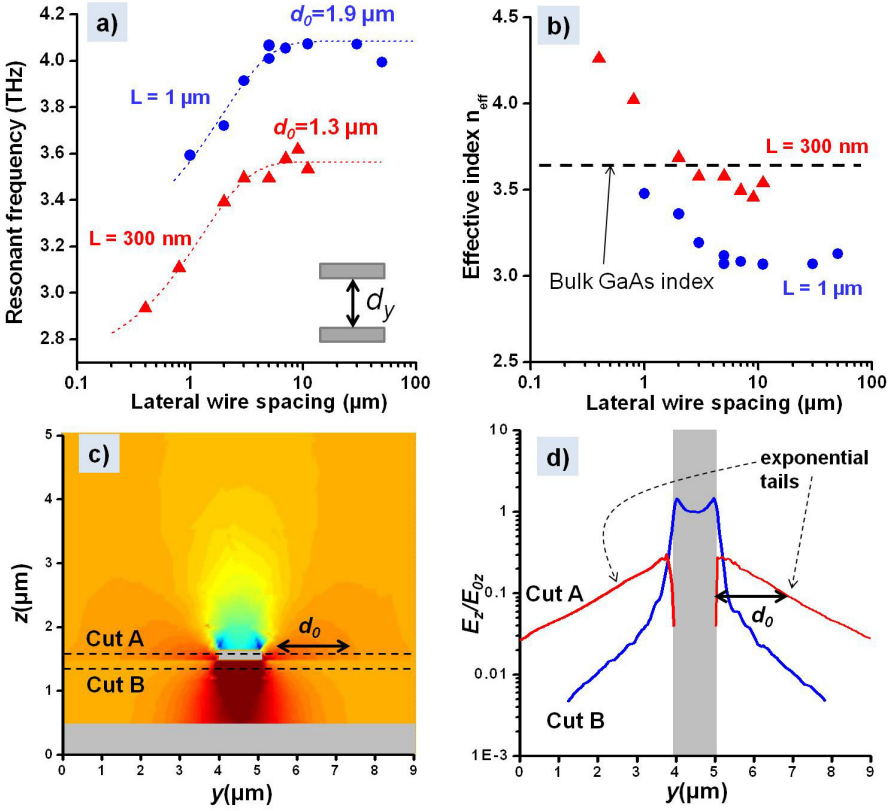

Fig. 3. (a) Measured resonant frequencies of micro-resonators with s = 12 µm and w = 1 µm, as a function of the lateral wire-wire gap d_y (logarithmic scale). The dashed lines are an exponential fit according to law $\nu = \nu_\infty - (\nu_\infty - \nu_0)\exp(-d_y / d_0)$. Circles: L = 1 µm, triangles: L = 300 nm. (b) The corresponding effective index as deduced from Eq. (1). The dashed line corresponds to the bulk GaAs index, n = 3.55. (c) Vertical electric field E_z for the L = 1 µm resonator (identical to Fig. 1(d)) with a color map saturated below the maximum field amplitude, in order to render visible the spreading fields in the y-direction. (d) Logarithmic plots of E_z (normalized to its maximal value E_{0z}) as a function of y along the two cuts A and B indicated in Fig. 3(c).

The physical meaning of the quantity d_0 is revealed by the numerical simulations of the L = 1 µm structure, presented in Figs. 3(c) and 3(d). Figure 3(c) is an enlarged version of the E_z plot of Fig. 1(d), where we have saturated the color map in order to render visible the spreading fields. This figure reveals very important field spreading in the plane of the metallic strip. In Fig. 3(d) we plot the variations of the field E_z as a function of y along to the cuts A an B defined in Fig. 3(c). The cut A correspond to the horizontal plane of the metallic strip, and the cut B corresponds to the region of strong field confinement, between the two metal layers. This plot shows that the field remains strongly confined under the stripe (cut B) and decays very fast away from the double-metal region. On the contrary, along the cut A, the field

#178514 - $15.00 USD Received 23 Oct 2012; revised 5 Dec 2012; accepted 5 Dec 2012; published 14 Dec 2012

features a slow decay away from the metallic edges. The variation of E_z in this region is very well fitted by an exponential decay law with d_0 = 1.5 μm, in fairly good agreement with the experimental data. Note from Fig. 3(d) that the amplitude of these exponential wings is almost an order of magnitude less than the amplitude of the field confined between the two metals, we therefore consider its contribution to the total energy density to be negligible. This was also confirmed from the numerical computation of the integral $\iint \varepsilon |E_z|^2 dydz$ from the 2D plots in Figs. 1(d) and 1(f). We have found that the contribution of the double region in this integral accounts for 85% for the L = 1 μm structure and for 97% for the L = 0.3 μm structure.

The effective index n_{eff} of the structures, deduced from Eq. (1), is plotted in Fig. 3(b), together with the bulk GaAs index (n = 3.55). This plot indicates that when the cavities are uncoupled, the effective index remains close, but inferior to the bulk index. The difference is stronger for the thicker structure: Δn = –0.5. This effect comes from a partial leak of the electric field in the air as the thickness is increased, as visible in the simulations in Fig. 1(c), 1(d). When the thickness of the devices is reduced the effective index is increased, reaching values close to the refractive index of the bulk core material due to a reduced leakage in the air, as clearly visible from the simulations in Fig. 1(e), 1(f). Therefore this study indicates that the electric field is well confined under stripe for structures with transverse aspect ratios $w/L > 1$.

3. Intersubband polaritons as a near field probe

When a microcavity mode of the wire-resonators described above is tuned into resonance with the intersubband (ISB) transition of quantum wells inserted inside the microcavity, the electronic polarization and the electromagnetic field enter the strong coupling regime, giving rise to two intersubband polariton states [13–15]. The energy separation between the polaritons, the Rabi splitting, is proportional to the square root of the spatial overlap between the electronic polarization and the electric field of the cavity mode. The polariton splitting can therefore be used as a precise near field probe of the electromagnetic confinement of the structure. To understand this point one has to recall that the electronic absorption between ISB levels is strongly anisotropic, and it is sensitive only to the electric field component parallel to the growth axis of the wells, the z-axis [20]. Therefore the ISB polarization is an effective tool to probe the dominant E_z component of the mode. The vacuum Rabi splitting is provided by the formula:

$$\Omega_R^2 = \Omega_0^2 \, \Psi^2 \qquad \text{with} \qquad \Omega_0^2 = \frac{e^2 f_{12} N_{2D} N_{QW}}{4 m^* \varepsilon \varepsilon_0 L} \tag{2}$$

where N_{QW} is the number of quantum wells inserted in the microcavity, N_{2D} is the population difference between the fundamental and excited subband of the QW expressed as sheet electron density, e is electron charge, m^* is the effective mass of the electrons, ε is the dielectric constant of the medium, and f_{12} is the oscillator strength for the transition. Note that in Eq. (2) the bare Rabi frequency is renormalized by the quantity Ψ^2, which is a geometrical factor, describing the spread of the electric field [21]:

$$\Psi^2 = \frac{\int_V E_z^2 d^3x}{\int_V (E_x^2 + E_y^2 + E_z^2) d^3x} \tag{3}$$

This quantity is the ratio between the electromagnetic energy contained in the z-component of the field and the total electromagnetic energy. For a perfect TM_0 mode of a double metal waveguide we have $\Psi^2 = 1$, whereas for more complex waveguide structures, that combine dielectric and metallic confinement, the typical value observed is $\Psi^2 = 0.5$ [21].

#178514 - $15.00 USD Received 23 Oct 2012; revised 5 Dec 2012; accepted 5 Dec 2012; published 14 Dec 2012

The structures that are closest to the ideal situation of almost zero field leakage are the stripe or square patch double-metal cavities [10,13]. We consider the latter as a reference where $\Psi^2 = 1$. We then compare the polariton splittings obtained from an identical QW medium, but processed once in square patch cavities, and once in the wire cavities to determine the spread factor Ψ^2 of the latter.

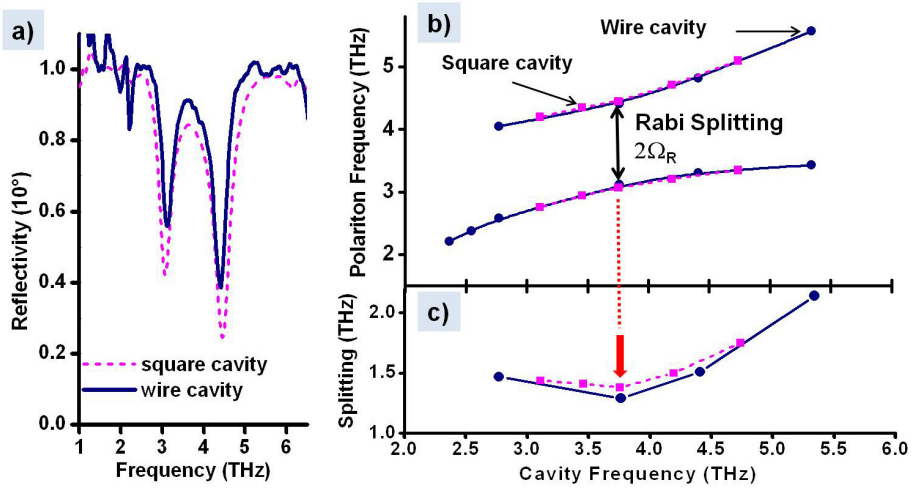

Fig. 4. (a) Typical polariton resonances obtained in low temperature reflectivity measurements for nearly resonant square (dotted curve) and wire cavity (solid curve) arrays. (b) Polariton frequencies measured for both type of structures as a function of the microcavity resonance. (c) Polariton splitting as a function of the cavity frequency. The minimal polariton splitting corresponds to the vacuum Rabi splitting $2\Omega_R$.

The core material for the cavities was GaAs/$Al_{0.15}Ga_{0.85}As$ hetero-structure similar to the design reported in Ref [13], with 32 nm wide quantum wells and 20 nm barriers. The structures were modulation doped in the barriers (5nm from the well). They contained a repeat of $N_{QW} = 25$ quantum wells, with an overall thickness $L = 1.3$ µm. The heterostructure was probed in multi-pass transmission measurements, that displayed a single 3.86 THz peak at $T = 4$ K. The peak corresponds to the transition between the two confined subbands of the well, with the electrons occupying dominantly the fundamental subband, with an estimated areal density of $N_{2D} = 1.7 \times 10^{11}$ cm^{-2} per quantum well.

The minimal energy splitting between the ISB polaritons can be inferred by measuring the polariton frequencies in cavities with variable detuning from the ISB resonance at 3.86 THz. For this purpose, both square patch and wire cavities with different length s between 6 µm and 20 µm were fabricated and measured. The width of the wires was $w = 1$µm. The results are summarized in Fig. 4.

Figure 4(a) reports on typical reflectivity spectra measured at low temperature. Instead of a single reflectivity dip, these spectra display two polariton dips corresponding to the cavity-ISB coupled polarization modes. In Fig. 4(b) we report on systematic studies of the polariton frequencies as a function of the frequency of the bare cavity resonance, measured at $T = 300$ K where the effect of the electronic absorption can be neglected. This measurements allow us to determine the minimal polariton splitting that corresponds to the vacuum Rabi splitting provided by Eq. (2) (Fig. 4(c)). From this data we deduce $2\Omega_R = 1.38$ THz for the square patch cavities and $2\Omega_R = 1.29$ THz for the wire microcavities. The slightly smaller (–6%) splitting observed for the wire type resonators, indicates more field leakage, with a spread factor of $\Psi^2 = 0.87$. This measurement confirms the strong confinement of the wire microcavities, despite the strongly reduced lateral size. Furthermore, the total number of electrons per well for these resonators was $1.1\text{x}10^4 - 3.9\text{x}10^4$ electrons per well, which is an

#178514 - $15.00 USD Received 23 Oct 2012; revised 5 Dec 2012; accepted 5 Dec 2012; published 14 Dec 2012

order of magnitude less than the typical values of $2x10^5$ required for square-patch resonators. These results indicate the potential of the concept of wire resonators for exploring the ultra-strong light-matter coupling regime with strongly reduced number of electronic dark states.

4. Summary and conclusion

In order to summarize the achievement of highly subwavelength volumes for the wire-resonator reported in this work, we use a dimensionless geometrical figure of merit that describes the light confinement:

$$R = \frac{(\lambda / 2n)^3}{V_{eff}} \tag{4}$$

where $V_{eff} = V_0/\Psi^2$ is the effective volume of the mode with $V_0 = swL$ the geometrical volume. We refer to Eq. (4) as a "squeezing factor", since it describes how a free propagating photon can be squeezed into a microcavity volume. In our wire-cavities only one dimension of the mode is commensurable with the wavelength in the material, therefore Eq. (4) becomes:

$$R = \frac{n_{eff}\Psi^2}{4wLn^3}\lambda^2 \tag{5}$$

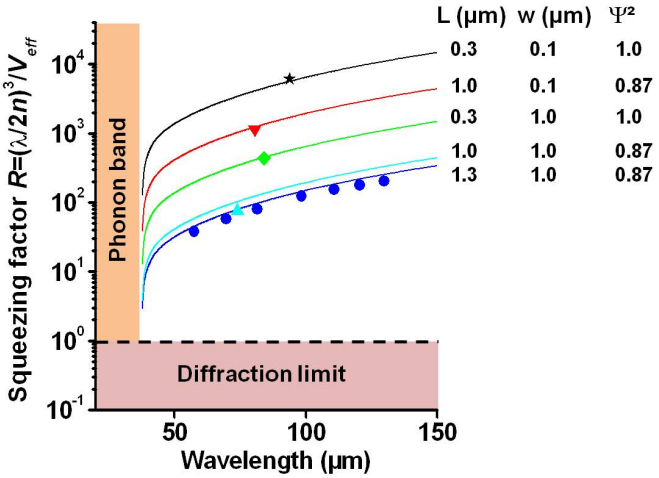

Fig. 5. Squeezing factor (Eq. (4) and Eq. (5)) as a function of the wavelength. The continuous lines are theoretical projections for perfect wire resonators, the dots report the cavities studied in this work. The rightmost column indicates the geometrical parameters of the structures.

The squeezing factors for the structures reported in this work, which operate exclusively in the THz domain, are summarized in Fig. 5. The continuous lines indicate the squeezing factor for ideal structures with perfect vertical confinement ($\Psi^2 = 1$) of electric field in a TM_{100} mode with $n_{eff} = n$. The dots correspond to the real structures. The values of L, w and Ψ^2 used in this plot have been reported in the right upper part of Fig. 5, next to each curve. To take into account the spreading fields we have used $\Psi^2 = 0.87$ for structures with $L \geq 1$ μm as measured from the polariton splitting (see previous section) . When $L = 0.3$ μm we estimate $\Psi^2 = 1.0$ due to the higher cavity effective index, n_{eff}, which increases the confinement. We have also taken into account the variations of the refractive index owing to the dispersion of the semiconductor. The highest value attained for our structures is $R = 6100$, well above the diffraction limit $R = 1$ that can be obtained in a dielectric cavity [22]. As a comparison, the squeezing factor for the structures with similar geometry reported in Ref [23]. is $R = 93$, and squeezing factors of $R = 225$ have been recently observed in the THz spectral range [3]. The

#178514 - $15.00 USD Received 23 Oct 2012; revised 5 Dec 2012; accepted 5 Dec 2012; published 14 Dec 2012

structures illustrated here have therefore an excellent figure of merit in terms of light confinement. This geometry may be of major interest for studying the ultra-strong coupling regime in a quantum semiconductor structures containing a low number of electrons.

The large light confinement also means an increased Purcell factor [24] for the spontaneous emission of sources inserted inside such microcavities. It is therefore interesting to comment on the possibility of such structures to being used for radiative enhancement of THz semiconductor sources [25, 26]. The Purcell factor can be expressed as $F_p = (6/\pi^2)RQ$, with Q the quality factor of the resonator. For the cavities with the highest R we have Q ~5.0, and a very high Purcell factor can be estimated F_p ~$2x10^4$. However, from the practical point of view, we need rather to evaluate the rate of photons collected outside the cavity, which can be estimated as F_pQ/Q_{rad}, where Q_{rad} represents the radiative quality factor of the wire microcavity. Regarding the structure as a microwave patch antenna, we can evaluate that Q_{rad} ~λ^2/wL [27], and therefore the increased confinement compensates exactly for the decreased radiative losses and there is no net benefit in terms of radiative efficiency. Indeed, in this case Q is dominated by the metal loss, and $Q_{rad} >> Q$. The benefit of the reduced cavity volume is more pertinent when regarding the structure as receiving antenna, rather than emitting one. In that case the Purcell factor measures the enhancement of the electromagnetic field energy density in the cavity with respect to the amplitude of the impinging wave. Such structures can therefore be useful for far-infrared detectors, with an increased ratio between photocurrent and dark current. This point will be developed elsewhere.

Acknowledgments

We gratefully acknowledge support from the French National Research Agency in the frame of its Nanotechnology and Nanosystems program P2N, Project No. ANR-09-NANO-007 and financial support from the ERC grant “ADEQUATE”.

#178514 - $15.00 USD Received 23 Oct 2012; revised 5 Dec 2012; accepted 5 Dec 2012; published 14 Dec 2012